European Journal of Mechanics B/Fluids 28 (2009) 259–270

Contents lists available at ScienceDirect

European Journal of Mechanics B/Fluids

www.elsevier.com/locate/ejmflu

Instability through porous media of three layers superposed conducting fluids

Kadry Zakaria, Magdy A. Sirwah, Sameh Alkharashi *

Mathematics Department, Faculty of Science, Tanta University, Tanta, Egypt

ARTICLE INFO

Article history:
Received 20 February 2008
Received in revised form 5 June 2008
Accepted 13 August 2008
Available online 20 August 2008

Keywords:
Kelvin–Helmholtz instability
Conducting fluids
Porous media

ABSTRACT

The instability properties of streaming superposed conducting fluids through porous media under the influence of uniform magnetic field have been investigated. The system is composed of a middle fluid sheet of finite thickness embedded between two semi-infinite fluids. The fluids are assumed to be incompressible, perfectly conducting and there are weak viscous stresses on the interfaces. The Rayleigh–Taylor and Kelvin–Helmholtz problems have been studied. Such configurations are of relevance in a variety of astrophysical and space configurations. The solutions of the linearized equations of motion together with the boundary conditions lead to deriving the dispersion equation with complex coefficients. The limiting case of the stability of one interface between two fluids has been discussed. The stability criteria are discussed theoretically and numerically in which stability diagrams are obtained. It has been found that the increase of the viscosity coefficient as well as the porosity plays a regular stabilizing role in the stability behavior, while the increase of the fluid velocity plays a destabilizing influence in the stability criteria.

1. Introduction

Magnetohydrodynamics (or MHD for short) is the macroscopic theory of electrically conducting fluids move in a magnetic field, providing a powerful and practical theoretical framework for describing both laboratory and astrophysical plasmas (a plasma is a hot, ionized gas containing free electrons and ions). The simplest example of an electrically conducting fluid is a liquid metal, for example, mercury or liquid sodium. However, the major use of MHD is in plasma physics. It is by no means obvious that plasmas can be regarded as fluids since the mean free paths for collisions between the electrons and ions are macroscopically long.

The instability of the plane interface between two superposed fluids with a relative horizontal velocity is called the Kelvin–Helmholtz instability. The linear theory governing the Kelvin–Helmholtz instability of a plane interface separating two superposed streaming fluids in MHD, when the fluids move with uniform speeds has been developed by Chandrasekhar [1]. The Kelvin–Helmholtz instability due to shear flow in stratified fluids has attracted the attention of many researchers because of its determinant influence on the stability of planetary and stellar atmospheres and in practical applications. The study of the Kelvin–Helmholtz instability has a long history in hydrodynamics. In the Kelvin–Helmholtz model, the effect of streaming is destabilizing through the linear approach. Lyon [2] added the effects of compressibility and electric field, but neglected the surface tension influence. Melcher [3] discussed the influence of both vertical and horizontal electric fields on Kelvin–Helmholtz incompressible flow in the presence of the surface tension effect.

The problems involving diffusion phenomena in fluids through porous media have been increasingly engaging the attention of many workers in last several decades. Such as geophysical fluid dynamicists [4,5], thermal and insulation engineering [6], the modeling of packed sphere beds, the cooling of electronic systems, groundwater hydrology, chemical catalytic reactors, ceramic processes, grain storage devices, fibre and granular insulation, petroleum reservoirs, coal combustors, ground water pollution and filtration processes, to name just a few of these applications. Sharma and Thakur [7] have studied the stability of the plane interface separating two viscous superposed conducting fluids through porous medium when the whole system is immersed in a uniform horizontal magnetic field. The stability analysis is carried out for two highly viscous fluids of equal kinematic viscosities. They found that the stability criterion is independent of the effects of viscosity and porosity of the medium and is dependent on the orientation and magnitude of the magnetic field. The magnetic field is found to stabilize a certain wave number range of the unstable configuration. Much of the work on this topic is reviewed by Nield and Bejan [8], Ingham and Pop [9], Vafai [10], and Pop and Ingham [11].

The instability of the plane interface between two uniform superposed fluids streaming through a porous medium was investigated by Sunil et al. [12]. They used linear stability analysis to obtain a characteristic equation for the growth rate of the disturbance and then solved this equation numerically. They concluded

* Corresponding author.
E-mail address: sameh7977@yahoo.com (S. Alkharashi).

0997-7546/$ – see front matter
doi:10.1016/j.euromechflu.2008.08.002

that Kelvin–Helmholtz instability is possible only if the heavier fluid is overlaying the lighter one (a statically unstable situation). This is obviously incorrect on physical grounds (possibly when Darcy's term is dominant). A series of studies for Kelvin–Helmholtz instability have been initiated by Gheorghitza [13], and Georgescu and Gheorghitza [14], where uniform motions of inviscid, incompressible fluids and heterogeneous porous media are considered in several simple cases.

Recently, Zakaria et al. [15] have studied the stability properties of time periodically streaming superposed magnetic fluids through porous media under the influence of an oblique alternating magnetic field. They found that the fluid sheet thickness plays a destabilizing role in the presence of a constant field and velocity while the damping role is observed for the resonant cases. Dual roles are observed for the fluid velocity and the porosity in the stability criteria.

The solution of such previous problems requires a knowledge of the details of the flow. One must know the magnitude and direction of the velocity at any point in the flow layers and also the effect of the porosity on the velocity and pressure distributions. In most previous studies on porous media, treatments based on Darcy's law and Forschheimer-extended Darcy's law models have been considered. However, it is well known that Darcy's law is an empirical formula relating the pressure gradient, the bulk viscous resistance and the gravitational force in a porous medium. In this case, the usual viscous term in the equation of motion is replaced by the resistive term $-(\tilde{\eta}/q)u$ where $\tilde{\eta}$ is the fluid viscosity, q is the medium permeability and u is the Darcian (filter) velocity of the fluid.

Many MHD problems of practical interest involving fluids as a working medium have attracted engineers, physicists and mathematicians alike. Some MHD problems have been discussed by El-Sayed [16] where the electrohydrodynamic instability of a plane layer of dielectric fluid which is in hydrostatic equilibrium between two semi-infinite conducting fluids with surface charges in porous media are investigated. He found (in Darcy model) that the electric field has a destabilizing effect, and both the surface tension and the liquid depth have stabilizing effects, while the fluid viscosity has a dual role (stabilizing and then destabilizing). In addition, El-Sayed [17] has studied the effects of collisions with neutral atoms on the hydrodynamic stability of the plane interface separating two streaming superposed composite plasmas of uniform densities in a porous medium. Korsunsky [18] has studied the propagation of weakly nonlinear waves over a flow of an electrically conducting viscous film flowing down an inclined plane under simultaneous action of electrical and magnetic fields. He found that the electrical field provides a destabilizing effect on the film flow while the magnetic field stabilizes it. Sunil and Singh [19] have studied the thermal instability of a Rivlin–Ericksen fluid in porous medium in the presence of a uniform vertical magnetic field to include the effect of Hall currents. For the case of stationary convection, the magnetic field has a stabilizing effect on the system, whereas the Hall currents have a destabilizing effect on the system. Attia and Sayed-Ahmed [20] have studied the unsteady MHD flow of an electrically conducting viscous incompressible non-Newtonian Bingham fluid bounded by two parallel nonconducting porous plates with heat transfer considering the Hall effect. An external uniform magnetic field is applied perpendicular to the plates and the motion of the fluid is subjected to a uniform suction and injection. They obtained numerical solutions for the governing momentum and energy equations taking the Joule and viscous dissipations into consideration. For additional other problems of MHD see Refs. [21–24].

The task of this work is to study the Kelvin–Helmholtz instability in three-dimensional motion for three conducting layers of fluids under the effect of a constant magnetic field with uniform velocity through porous media. The field and the stream are inclined in the horizontal plane. The organization of this paper is as follows: In Section 2, we give a description of the problem including the basic equations of the fluid mechanics and Maxwell's equations governing the motion of our model. This section contains also the equilibrium solutions, the appropriate boundary conditions and linear perturbation. Section 3 is concerned with the derivation of the characteristic equations and numerical estimation for stability configuration in the presence of the constant magnetic field. Some stability diagrams are plotted and discussed. Also in this section, the Rayleigh–Taylor instability is investigated as a special case of non-streaming model. In Section 4, the limiting case of the stability of one interface has been discussed, while the final section is devoted to the conclusions.

2. The problem statement

2.1. Governing equations and linear perturbations

We consider the motion of two semi-infinite superposed fluids separated by a middle layer of depth $2a$, through porous media. The fluids are assumed to be incompressible and perfectly conducting, and there are weak viscous stresses on the interfaces. There are two interfaces between the fluids are assumed to be well defined and initially flat and forms the planes $z=-a$ and $z=a$. In fact, sharp interfaces between the fluids may not exist. Rather, there is an ill-defined transition region in which the two fluids intermix. The width of this transition zone is usually small compared with the other characteristic length of the motion; hence, for the purpose of the mathematical analysis, we shall assume that the fluids are separated by sharp interfaces. The two planes are parallel and the flow in each phase is everywhere parallel to each other. The surfaces deflection is expressed by $z=\xi_1(x,y,t)$ at $z=a$ and $z=\xi_2(x,y,t)$ at $z=-a$ propagated in the xy-plane, where x, y, and z are Cartesian co-ordinates referred to axes such that $z=0$ is the mid-plane of the intermediate layer and the positive z-axis is measured vertically upwards. The unit vectors e_x, e_y and e_z are in the x, y and z directions, respectively (the geometry of the flow is depicted in Fig. 1). The fluid with density ρ_1 occupies the space $z>a$, the region typified by $-a<z<a$, has density ρ_2 whereas $z<-a$ is occupied by the fluid with density ρ_3 and the acceleration due to gravity, acts vertically downward, is given by $(0,0,g)$. The system is subject to a magnetic field permeates the fluids before disturbance which is given by $(H_1,H_2,0)$ and acts in the xy-plane. The fluids are moving with uniform velocity $(U_1,U_2,0)$, such that:

$$\boldsymbol{U}^{(j)}=U_1^{(j)}\boldsymbol{e}_x+U_2^{(j)}\boldsymbol{e}_y,\quad j=1,2,3, \tag{1}$$

$$\boldsymbol{H}^{(j)}=H_1^{(j)}\boldsymbol{e}_x+H_2^{(j)}\boldsymbol{e}_y=H_0^{(j)}\cos\theta\boldsymbol{e}_x+H_0^{(j)}\sin\theta\boldsymbol{e}_y. \tag{2}$$

The superscripts $j=1,2,3$ refer to quantities in the upper fluid, intermediate layer and lower fluid respectively and θ is the angle in the xy-plane.

The required fundamental equations for analyzing and describing such kind of problems are coming out from the combination of Maxwell's electromagnetic equations together with the ordinary hydrodynamic equations [25,26]. In fact, we shall often use dimensionless variables in order to understand hydrodynamic stability better. We shall use an asterisk as a superscript to the dimensional form and omit the asterisk for the dimensionless form where it is desirable to use the forms of the same physical quantities. Sometimes we shall need only the dimensional form and so shall not use the asterisks. Thus, we may henceforth write $u^*(x^*,t^*)$ for the dimensional and $u(x,t)$ for the dimensionless total velocity of a disturbed flow. The surface disturbance $\xi^*=a\xi$, the stream velocity $U^*=\sqrt{ag}U$, the time $t^*=\sqrt{a/g}t$, the pressure $p^*=ag\rho_2 p$, the

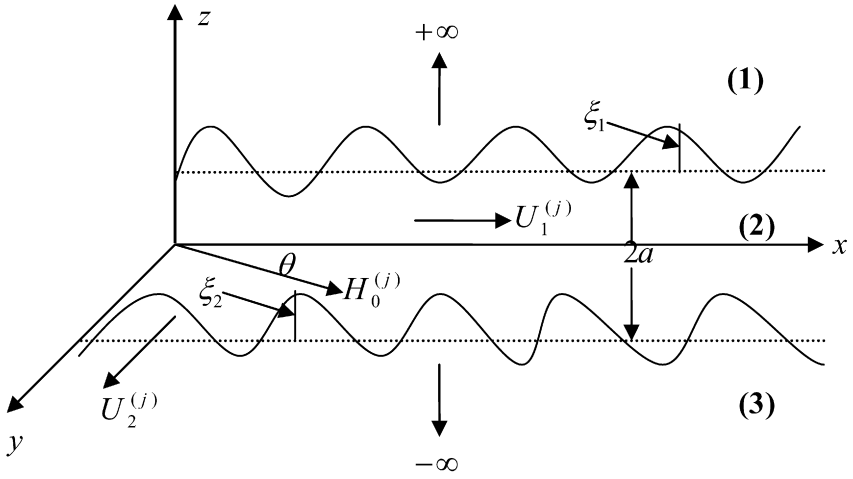

Fig. 1. The geometry of the problem.

magnetic field $H^* = \sqrt{ag\rho_2/\mu_2}H$, the porosity $\tilde{\sigma}^* = \rho_2\sqrt{g/a}\tilde{\sigma}$, the viscosity $\eta^* = \rho_2\sqrt{a^3 g}\eta$, and $(x^*, y^*, z^*) = a(x, y, z)$.

And by using the symbols $\hat{\rho}_j = \rho_j/\rho_2$ $(j = 1, 2, 3)$, $W_l = T_l/a^2\rho_2 g$ $(l = 1, 2)$ in the equations of motion, where W_l is the Weber number and T_l is the surface tension coefficient. In addition, we use the assumption $\boldsymbol{h} = \sqrt{\mu/\rho}\boldsymbol{H}$ (units of velocity).

Under the present circumstances, these equations may be formulated in the dimensionless form as follows:

The hydromagnetic vector equation of motion that governs the motion of conducting fluid through porous media is

$$\frac{D\boldsymbol{u}^{(j)}}{Dt} = -\nabla\pi^{(j)} - \frac{\tilde{\sigma}_j}{\hat{\rho}_j}\boldsymbol{u}^{(j)} + (\boldsymbol{h}^{(j)}.\nabla)\boldsymbol{h}^{(j)}, \quad j = 1, 2, 3, \tag{3}$$

where

$$\pi^{(j)} = \frac{p^{(j)}}{\hat{\rho}_j} + z + \frac{1}{2}h^{(j)^2}, \tag{4}$$

is the total pressure on the interfaces, $D/Dt \equiv \partial/\partial t + (u.\nabla)$ stands for the convective derivative, $\partial/\partial t$ is the partial derivative with respect to time, $\nabla \equiv (d/dx, d/dy, d/dz)$ is the gradient operator and p refers to the fluid pressure.

We denote the porosity by $\tilde{\sigma}_j = \tilde{\eta}_j/q_j$ which is also called Darcy coefficient [15], where the parameters $\tilde{\eta}_j$ and q_j are the fluid viscosity and permeability of the porous media, respectively.

The equation of continuity appropriate for incompressible fluid is

$$\nabla.\boldsymbol{u}^{(j)} = 0, \tag{5}$$

expressing the conservation of mass.

The equation expressing the conservation of flux

$$\nabla.\boldsymbol{h}^{(j)} = 0, \tag{6}$$

which is identically satisfied for any magnetic field of any intensity.

The evolution equation of motion of magnetic field is

$$\frac{\partial\boldsymbol{h}^{(j)}}{\partial t} = (\boldsymbol{h}^{(j)}.\nabla)\boldsymbol{u}^{(j)} - (\boldsymbol{u}^{(j)}.\nabla)\boldsymbol{h}^{(j)}. \tag{7}$$

Here $\boldsymbol{u}$ is the total fluid velocity given by

$$\boldsymbol{u}^{(j)} = \boldsymbol{U}^{(j)} + \boldsymbol{V}^{(j)}(x, y, z, t), \tag{8}$$

where $\boldsymbol{V}^{(j)} = (u^{(j)}, v^{(j)}, w^{(j)})$ is the perturbed velocity and $\boldsymbol{h}$ is the total magnetic field vector given by

$$\boldsymbol{h}^{(j)} = \boldsymbol{H}^{(j)} + \boldsymbol{h}_1^{(j)}(x, y, z, t), \tag{9}$$

where $\boldsymbol{h}_1^{(j)} = (h_x^{(j)}, h_y^{(j)}, h_z^{(j)})$ is the perturbed field.

To investigate the stabilization of the present problem, the interfaces between the fluids will be assumed to be perturbed about its equilibrium location and will cause a displacement of the material particles of the fluid system. Analyzing the perturbations into normal modes, we assume that the perturbed quantities have a space and time dependence of the form

$$f(z)\exp(ik_1x + ik_2y + \omega t), \tag{10}$$

where k_1, k_2 are the wave numbers along the x and y directions respectively (horizontal wave numbers), $k = \sqrt{k_1^2 + k_2^2}$ is the resultant wave number of the disturbance ($k = 2\pi/\lambda$, where λ is the wavelength of the disturbance), ω is the growth rate of the harmonic disturbance which is, in general, a complex constant ($\omega = \omega_r + i\omega_i$ where ω_r represents the rate of growth of the disturbance, ω_i is 2π times the disturbance frequency), and $f(z)$ is some function of z.

The deformation in the planes $z = \pm 1$ are due to the perturbation about the equilibrium values for all the other variables. The equations of motion and the boundary conditions mentioned previously will be solved for these perturbations under the assumption that the perturbations are small, that is, all equations of motion and boundary conditions will be linearized in the perturbed quantities. The form of horizontal variation for all the other perturbed variables will be the same as the displacement description (10). Perturbation bulk variables are functions of both the horizontal and vertical co-ordinates as well as time.

In accordance with the interface deflecting given by (10) and in view of a standard Fourier decomposition, we may similarly assume that the bulk solutions are periodic functions in x, y and exponential functions in t, which are regarded as:

$$\begin{aligned}
&\xi_l(x, y, t) = \hat{\xi}_l\exp(ik_1x + ik_2y + \omega t) + c.c,\\
&\boldsymbol{h}_1^{(j)}(x, y, z, t) = \hat{\boldsymbol{h}}_1^{(j)}(z)\exp(ik_1x + ik_2y + \omega t) + c.c,\\
&\boldsymbol{V}^{(j)}(x, y, z, t) = \hat{\boldsymbol{V}}^{(j)}(z)\exp(ik_1x + ik_2y + \omega t) + c.c,
\end{aligned} \tag{11}$$

where $\hat{\xi}_l$ is the initial amplitude of the disturbance, which is taken to be much smaller than the half-thickness a of the sheet, the symbol i denotes $\sqrt{-1}$, the imaginary number, and $c.c$ stands for the complex conjugate of the preceding terms.

2.2. Boundary conditions and solutions

The flow field solutions of the above governing equations have to satisfy the kinematic and dynamic boundary conditions at the two planes. At the boundaries among fluids, the fluids and the

magnetic stresses must be balanced. The components of these stresses consist of the hydrodynamic pressure, surface tension, porosity effects and magnetic stresses [27,28]. These boundary conditions represented here are prescribed at the planes $z = \xi_l(x, y, t)$. As the interfaces are deformed all variables are slightly perturbed from their equilibrium values. Because the interfacial displacement is small, the boundary conditions on perturbation interfacial variables need to be evaluated at the equilibrium position rather than at the interface. Therefore, it is necessary to express all the physical quantities involved in terms of Taylor series about $z = \pm 1$.

(i) Kinematics condition that the normal component of the velocity vector in each of the phases of the system is continuous at the dividing surface. This implies that

$$\boldsymbol{n}_l.\boldsymbol{u}^{(l)} = \boldsymbol{n}_l.\boldsymbol{u}^{(l+1)}, \qquad z = (-1)^{l+1}, \quad l = 1, 2, \tag{12}$$

where $\boldsymbol{n}_l$ is the outward normal unit vector to the interfaces which is given from the relation, $\boldsymbol{n}_l = \nabla F_l/|\nabla F_l|$, and $F_l(x, y, z, t)$ is the surface geometry.

(ii) The kinematic condition will be

$$w^{(l),(l+1)} = \frac{\partial \xi_l}{\partial t} + U_1^{(l),(l+1)} \frac{\partial \xi_l}{\partial x} + U_2^{(l),(l+1)} \frac{\partial \xi_l}{\partial y},$$
$$z = (-1)^{l+1}, \quad l = 1, 2. \tag{13}$$

(iii) The continuity of the normal component of the magnetic displacement at the interface gives

$$\boldsymbol{n}_l.\boldsymbol{h}^{(l)} = \boldsymbol{n}_l.\boldsymbol{h}^{(l+1)}, \qquad z = (-1)^{l+1}, \quad l = 1, 2. \tag{14}$$

(iv) The normal component of the stress tensor is discontinuous by the amount of the surface tension [29]. Thus, the balance at the dividing surfaces gives

$$\left|[\boldsymbol{n}_l.\boldsymbol{\tau}.\boldsymbol{n}_l]\right|_l^{l+1} = -W_{l(l+1)} \nabla.\boldsymbol{n}_l,$$
$$z = \pm 1 + \xi_l(x, y, t), \quad l = 1, 2, \tag{15}$$

where $T_{l(l+1)}$ is the surface tension through the surfaces separating fluid l from fluid $l+1$, τ is the viscous stress tensor at the interfaces given by

$$\tau_{mn} = -\pi \delta_{mn} + \eta\left(\frac{\partial u_m}{\partial x_n} + \frac{\partial u_n}{\partial x_m}\right), \tag{16}$$

δ_{mn} is the Kronecker's delta, η is the coefficient of viscosity.

To determine the perturbed pressure $\pi_1^{(j)}$, we take the divergence of Eq. (3). Thus we obtain Laplace's equation (up to first order) such that

$$\nabla^2 \pi_1^{(j)} = 0, \tag{17}$$

since the boundary conditions require that the disturbances vanish as $z \to \pm\infty$. Thus the solution of Eq. (17) is

$$\pi_1^{(1)} = A_1^{(1)} e^{-kz} \exp(ik_1 x + ik_2 y + \omega t) + c.c, \quad z > 1,$$
$$\pi_1^{(2)} = \left(A_1^{(2)} e^{-kz} + A_2^{(2)} e^{kz}\right) \exp(ik_1 x + ik_2 y + \omega t)$$
$$+ c.c, \quad -1 < z < 1,$$
$$\pi_1^{(3)} = A_2^{(3)} e^{kz} \exp(ik_1 x + ik_2 y + \omega t) + c.c, \quad z < -1, \tag{18}$$

where $A_1^{(j)}$ and $A_2^{(j)}$ are integration constants, to be determined from the above conditions and given in Appendix A(I). Solving the system of Eqs. (3)–(7), we get

$$u^{(j)} = \frac{-ik_1 (A_1^{(j)} e^{-kz} + A_2^{(j)} e^{kz}) \exp(ik_1 x + ik_2 y + \omega t)}{F^{(j)} \hat{\rho}_j^{-1} \tilde{\sigma}_j + F^{(j)^{-1}} (k_1 H_1^{(j)} + k_2 H_2^{(j)})^2}, \tag{19}$$

$$v^{(j)} = \frac{-ik_2 (A_1^{(j)} e^{-kz} + A_2^{(j)} e^{kz}) \exp(ik_1 x + ik_2 y + \omega t)}{F^{(j)} \hat{\rho}_j^{-1} \tilde{\sigma}_j + F^{(j)^{-1}} (k_1 H_1^{(j)} + k_2 H_2^{(j)})^2}, \tag{20}$$

$$w^{(j)} = \frac{(kA_1^{(j)} e^{-kz} - kA_2^{(j)} e^{kz}) \exp(ik_1 x + ik_2 y + \omega t)}{F^{(j)} \hat{\rho}_j^{-1} \tilde{\sigma}_j + F^{(j)^{-1}} (k_1 H_1^{(j)} + k_2 H_2^{(j)})^2}, \tag{21}$$

$$\left(h_x^{(j)}, h_y^{(j)}, h_z^{(j)}\right) = F^{(j)^{-1}} i\left(k_1 H_1^{(j)} + k_2 H_2^{(j)}\right)\left(u^{(j)}, v^{(j)}, w^{(j)}\right), \tag{22}$$

where $F^{(j)} = (\omega + ik_1 U_1^{(j)} + ik_2 U_2^{(j)})$.

3. Derivation of the characteristic equations and their stability

3.1. Dispersion equation

In this section, we shall determine the boundary-value problem. It constitutes a homogeneous system of equations and boundary conditions, cited above to explain the factors governing the surface wave's propagation. Inserting Eqs. (18)–(22) into the dynamical conditions (15), finally we obtain the following characteristic equation

$$\omega^4 + (\alpha_1 + i\alpha_2)\omega^3 + (\alpha_3 + i\alpha_4)\omega^2 + (\alpha_5 + i\alpha_6)\omega + \alpha_7 + i\alpha_8 = 0, \tag{23}$$

where the coefficients α's are defined in Appendix A(II).

Eq. (23) is the desired dispersion relation of the MHD stability of a conducting layer embedded between two other conducting fluids with the influence of constant magnetic field and uniform stream, through porous media. The relation (23) contains the most stability information of MHD flow under the influence of weak viscous stresses on the interfaces among the fluids. All the roots of Eq. (23) will have negative real parts, and hence the corresponding system is stable as the following conditions are satisfied [15,30]

$$\kappa_1 > 0, \quad \kappa_2 > 0, \quad \kappa_3 > 0, \quad \kappa_4 \geqslant 0, \tag{24}$$

where κ_m, $m = 1, \ldots, 4$, are given in Appendix A(III). Conditions (24) can be arranged and rewritten in the form

$$\breve{\kappa}_1 H_0^{(1)^2} + \breve{\kappa}_2 > 0,$$
$$\hat{\kappa}_1 H_0^{(1)^4} + \hat{\kappa}_2 H_0^{(1)^2} + \hat{\kappa}_3 > 0,$$
$$\tilde{\kappa}_1 H_0^{(1)^6} + \tilde{\kappa}_2 H_0^{(1)^4} + \tilde{\kappa}_3 H_0^{(1)^2} + \tilde{\kappa}_4 \geqslant 0, \tag{25}$$

subject to $\alpha_1 > 0$ or $(1/L_0)(L_{11}L_{22} + L_{12}L_{22} - M_{11}M_{22} - M_{12}M_{21}) > 0$, where the coefficients $\breve{\kappa}_l$ $(l = 1, 2)$, $\hat{\kappa}_j$ $(j = 1, 2, 3)$ and $\tilde{\kappa}_m$ $(m = 1, \ldots, 4)$ are clear form the context.

3.2. Rayleigh–Taylor instability

The stability analysis of the model can be classified according to the initial state i.e. according to the streaming velocities of the fluids. In the limiting case of the nonstreaming fluids (the linear stability of the Rayleigh–Taylor problem for general surface deflections, when $U_0^{(j)} = 0$), the dispersion relation (23) reduces to

$$\omega^4 + \hat{\alpha}_1 \omega^3 + \hat{\alpha}_3 \omega^2 + \hat{\alpha}_5 \omega + \hat{\alpha}_7 = 0, \tag{26}$$

where the coefficients $\hat{\alpha}_r = \alpha_r$ $(r = 1, 3, 5, 7)$ as $U_0^{(j)} = 0$. The relation (26) contains the most stability information of the nonstreaming model. In view of Hurwitz criterion [31], the system characterized by (26) will be stable when

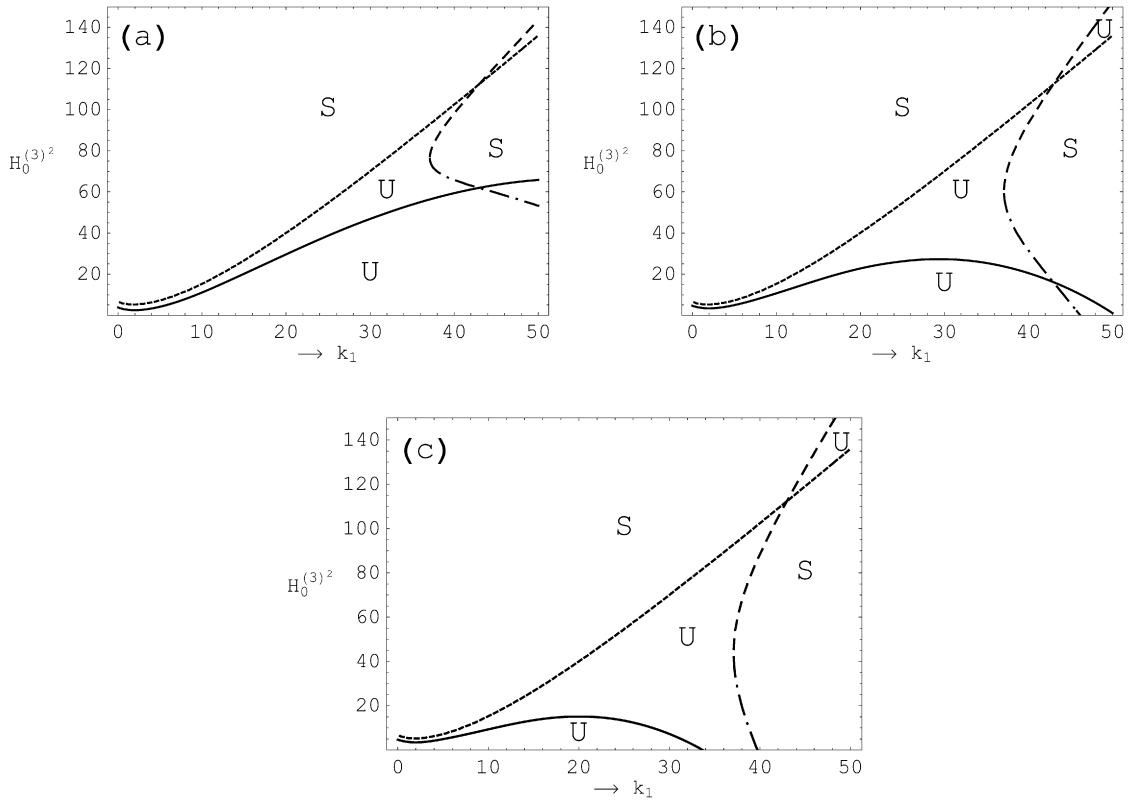

Fig. 2. The stability diagrams according to Eqs. (29). The graph construction is based on the stability conditions (28), for a system having the parameters $H_0^{(1)} = 3$, $H_0^{(2)} = 1$, $\tilde{\sigma}_1 = 2$, $\tilde{\sigma}_2 = 3$, $\tilde{\sigma}_3 = 1$, $\eta_1 = 1$, $\eta_2 = 0.5$, $k_2 = 5$, $\theta = 45$, $\hat{\rho}_1 = 50$, $\hat{\rho}_3 = 5$, $W_1 = 8$ and $W_2 = 10$ with $\eta_3 = 0.2$, 1 and 1.8 of the partitions (a), (b) and (c), respectively.

$$\hat{\alpha}_1\hat{\alpha}_3 - \hat{\alpha}_5 \geqslant 0,$$
$$\hat{\alpha}_5(\hat{\alpha}_1\hat{\alpha}_3 - \hat{\alpha}_5) - \hat{\alpha}_1^2\hat{\alpha}_7 > 0,$$
$$\hat{\alpha}_7 > 0 \tag{27}$$

are satisfied. Relations (27) can be written in the form

$$N_{11}H_0^{(3)^2} + N_{12} \geqslant 0,$$
$$N_{21}H_0^{(3)^2} + N_{22}H_0^{(3)^2} + N_{23} > 0,$$
$$N_{31}H_0^{(3)^2} + N_{32} > 0, \tag{28}$$

where the coefficients that appeared in these relations are clear from the context. Conditions (28) will give four possible transition curves in the plane $(H_0^{(3)^2}$–$k_1)$, which are

$$H_{01}^{(3)^2} = \frac{-N_{12}}{N_{11}}, \qquad H_{02}^{(3)^2} = \frac{-N_{32}}{N_{31}},$$
$$H_{03}^{(3)^2} = \frac{-N_{22} + \sqrt{N_{22}^2 - 4N_{21}N_{23}}}{2N_{21}},$$
$$H_{04}^{(3)^2} = \frac{-N_{22} - \sqrt{N_{22}^2 - 4N_{21}N_{23}}}{2N_{21}}. \tag{29}$$

These transition curves separate the stable region from the unstable one, which are determined by the validity of the stability conditions (28). In other words, the wave under consideration will only be stable if all the conditions of (28) are satisfied, and otherwise the surface waves will be unstable. In order to discuss the stability diagrams, Eq. (26) is used to control the stability behavior. Numerical calculations for the transition curves (29) are displayed in Figs. 2 and 3. A numerical search was conducted to seek three consequent values for each parameter displayed in these graphs for comparison. The stable region involved in these graphs was decided by satisfying the inequalities (28) of the stability conditions, where S represents the stable region and U indicates the unstable case. The stability examination is performed by fixing the value of all the physical parameters except for one parameter having varying values for comparison. Fig. 2 represents the influence of the viscosity coefficient η_3 in the plane $(H_0^{(3)^2}$–$k_1)$, for a system having the dimensionless parameters $H_0^{(1)} = 3$, $H_0^{(2)} = 1$, $\tilde{\sigma}_1 = 2$, $\tilde{\sigma}_2 = 3$, $\tilde{\sigma}_3 = 1$, $\eta_1 = 1$, $\eta_2 = 0.5$, $k_2 = 5$, $\theta = 45$, $\hat{\rho}_1 = 50$, $\hat{\rho}_3 = 5$, $W_1 = 8$ and $W_2 = 10$. In Fig. 2(a), we choose a suitable value of η_3 to be 0.2, the stable region lies between the intersection of the four curves $H_{0m}^{(3)^2}$, $m = 1, \ldots, 4$, the stable region lies above and under the curves. In view of the stability conditions (28), the stability diagram shown in this graph represents four regions, two of them are stable and the others are unstable. In Fig. 2(b), the value of the viscosity η_3 is increased to be 1. By examining the parts (a) and (b) of Fig. 2 we observe that the stable regions are increased while the unstable regions are decreased. In Fig. 2(c), the viscosity changes from $\eta_3 = 1$ to $\eta_3 = 1.8$. By comparing parts (a)–(c) of Fig. 2, we found that the stable regions are enlarged when the viscosity increases, i.e. the increase in the values of the viscosity changes the unstable waves into stable waves. Hence, we deduce that the viscosity coefficient η_3 plays a stabilizing role in the movement of the waves in the lower fluid. This regular influence may be physically interpreted as a part of the kinetic energy of the waves has been absorbed, which leads to damping in the frequency of the waves.

The effect of the viscosity coefficient of the upper fluid is investigated in the parts (a–b) of Fig. 3 in which the plane $(H_0^{(3)^2}$–$k_2)$ is divided into stable and unstable regions and represented by two lines of the transition curves given by relations (29). The inspection of the stability conditions (28) reveals that the lower region and the area bounded by the two transitions curves (the dotted and dashed lines) are unstable while the upper region is stable. In

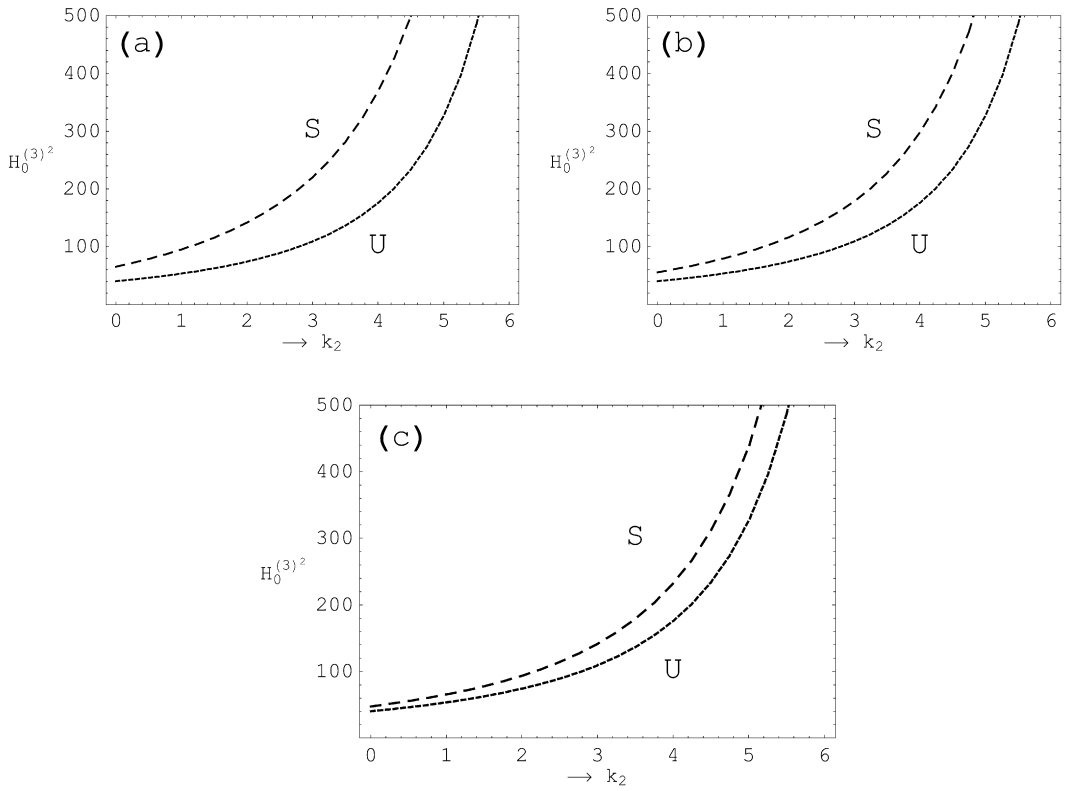

Fig. 3. Influence of the variation of the viscosity on the stability picture for a system having the parameters $H_0^{(1)} = 5$, $H_0^{(2)} = 8$, $\tilde{\sigma}_1 = 3$, $\tilde{\sigma}_2 = 5$, $\tilde{\sigma}_3 = 1$, $\eta_2 = 1.5$, $\eta_3 = 2.5$, $k_1 = 50$, $\theta = 30$, $\hat{\rho}_1 = 20$, $\hat{\rho}_3 = 50$, $W_1 = 1$, $W_2 = 2$ with $\eta_1 = 0.01, 1$ and 4 of the parts (a), (b) and (c), respectively.

Fig. 3(a) we fixed the quantities $H_0^{(1)} = 5$, $H_0^{(2)} = 8$, $\tilde{\sigma}_1 = 3$, $\tilde{\sigma}_2 = 5$, $\tilde{\sigma}_3 = 1$, $\eta_2 = 1.5$, $\eta_3 = 2.5$, $k_1 = 50$, $\theta = 30$, $\hat{\rho}_1 = 20$, $\hat{\rho}_3 = 50$, $W_1 = 1$, $W_2 = 2$ and take $\eta_1 = 0.01$. In Fig. 3(b) the value of η_1 is increased to 1 under the same parameters given in the part (a) of Fig. 3. By checking the stability conditions (28), we determine the stable and unstable regions. It is found that there is an extension in the stable region, while, there is a contraction in the instability areas. In Fig. 3(c), we repeated the calculations in part (a) of Fig. 3 with a change in the value of the viscosity coefficient $\eta_1 (= 4)$. Studying the stable and unstable regions, lead to the conclusion that the increase of the viscosity coefficient η_1 increases the stable region while decreases the unstable regions. The comparison between the graphs (a)–(c) of Fig. 3 shows that the effect of the viscosity in the upper fluid has a regular stabilizing influence on the movement of the waves where the increase of the values of the viscosity has changed the unstable waves into stable waves.

3.3. Kelvin–Helmholtz instability

The Kelvin–Helmholtz instability is very important in understanding a variety of space and astrophysical phenomena involving sheared plasma flow such as the stability of the interface between the solar wind and magnetosphere, interaction between adjacent streams of different velocities in the solar wind [31]. Once more, we return to the general form of the dispersion relation (23) which is used to control the stability behavior for the fluid sheet. In graphing the stability picture, numerical computations are made for the stability conditions (25). From these conditions we can similarly as in the above case of Rayleigh–Taylor instability obtain the transition curves and discuss the stability behavior. In parts of Fig. 4, we investigate the influence of changes of the streaming velocity $U_2^{(2)}$ on the stability picture, three values of $U_2^{(2)}$ are collected in Fig. 4 in the plane $(H_0^{(1)^2} - \eta_1)$, for a system having the dimensionless parameters $H_0^{(2)} = 1$, $H_0^{(3)} = 5$, $U_1^{(1)} = 8.7$, $U_2^{(1)} = 5$, $U_1^{(2)} = 0.5$, $U_1^{(3)} = 0.85$, $U_2^{(3)} = 0.5$, $k_1 = 0.02$, $k_2 = 5$, $\tilde{\sigma}_1 = 8$, $\tilde{\sigma}_2 = 3$, $\tilde{\sigma}_3 = 0.5$, $\eta_2 = 0.4$, $\eta_3 = 0.005$, $\theta = 60$, $\hat{\rho}_1 = 10$, $\hat{\rho}_3 = 20$, $W_1 = 8$ and $W_2 = 10$. In Fig. 4(a) we select the value of the velocity in the inner layer $U_2^{(2)} = 50$, and check the stability conditions (25) to determine the regions of stable and unstable motion. We noticed that the (in)stability domain is partitioned to five areas of stable and unstable regions, two of these areas are unstable and the others are stable. The part (b) of Fig. 4 is considered to the velocity value $U_2^{(2)} = 60$. Having checked the stability picture of the parts (a) and (b) of Fig. 4, it is discovered that further increasing of the streaming velocity leads to more increase in the width of each of the region unstable regions while there is a contraction in the stable regions. In Fig. 4(c), we repeated the same diagrams as illustrated in Figs. 4 (a) and (b) with a change in the value of the velocity $U_2^{(2)}$ to be 70. Under this change of the velocity, further increases in the unstable regions while the stable regions decreases. A conclusion that may be made from the comparison among the parts (a)–(c) of Fig. 4 is that the streaming velocity does not have a regular influence on the stability behavior of the movement of the fluids. In other words, this result can be physically interpreted that there is an increasing of the kinetic energy of the particles of the fluids. This is due to the increasing of the streaming velocity, which leads to an increasing in the perturbed motions. Fig. 5 is sketched in the plane $(H_0^{(1)^2} - \eta_1)$ for three different values of the porosity of the upper fluid layer where we fixed the other parameters as $H_0^{(2)} = 1$, $H_0^{(3)} = 0.1$, $U_1^{(1)} = 0.09$, $U_2^{(1)} = 0.05$, $U_1^{(2)} = 4.5$, $U_2^{(2)} = 2.5$, $U_1^{(3)} = 0.85$, $U_2^{(3)} = 0.5$, $k_1 = 1$, $k_2 = 5$, $\tilde{\sigma}_2 = 3$, $\tilde{\sigma}_3 = 1$, $\eta_2 = 0.5$, $\eta_3 = 0.5$, $\theta = 60$, $\hat{\rho}_1 = 1$, $\hat{\rho}_3 = 2$, $W_1 = 8$ and $W_2 = 10$. To screen the role of the increasing of the porosity in the stability profile we take $\tilde{\sigma}_1 = 2$, in Fig. 5(a). Inspection of stability diagram by using the truth of the inequalities

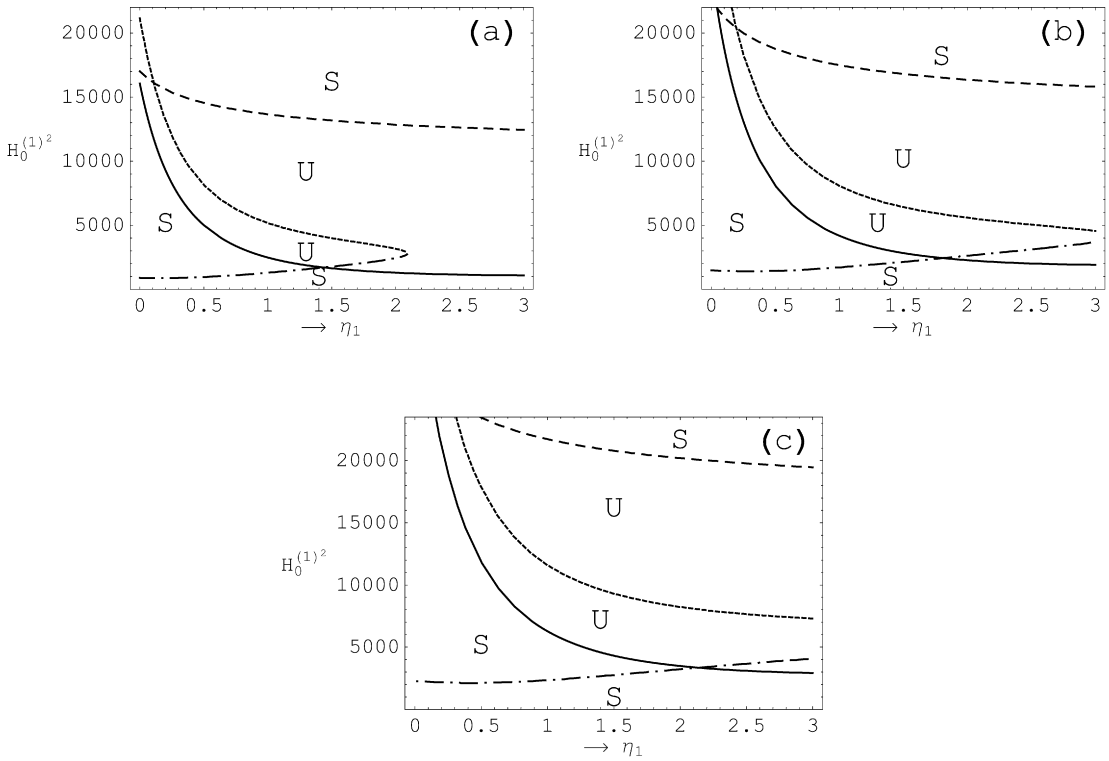

Fig. 4. The stability diagrams in the plane $(H_0^{(1)^2}-\eta_1)$, according to the transition curves represented by relations (25) for a system having $H_0^{(2)}=1$, $H_0^{(3)}=5$, $U_1^{(1)}=8.7$, $U_2^{(1)}=5$, $U_1^{(2)}=0.5$, $U_1^{(3)}=0.85$, $U_2^{(3)}=0.5$, $k_1=0.02$, $k_2=5$, $\tilde{\sigma}_1=8$, $\tilde{\sigma}_2=3$, $\tilde{\sigma}_3=0.5$, $\eta_2=0.4$, $\eta_3=0.005$, $\theta=60$, $\hat{\rho}_1=10$, $\hat{\rho}_3=20$, $W_1=8$ and $W_2=10$ with $U_2^{(2)}=50, 60$ and 70 of the partitions (a), (b) and (c), respectively.

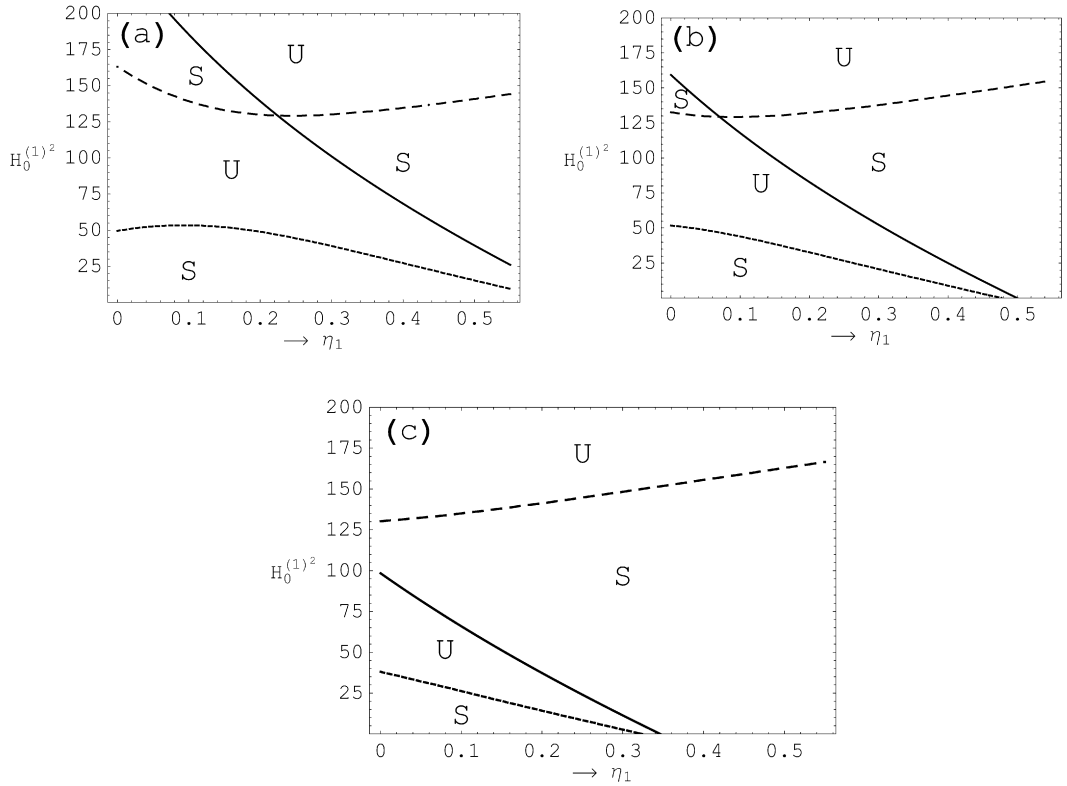

Fig. 5. The graphs are constructed for $H_0^{(1)^2}$ against η_1 according to relations (25) for a system having the parameters $H_0^{(2)}=1$, $H_0^{(3)}=0.1$, $U_1^{(1)}=0.09$, $U_2^{(1)}=0.05$, $U_1^{(2)}=4.5$, $U_2^{(2)}=2.5$, $U_1^{(3)}=0.85$, $U_2^{(3)}=0.5$, $k_1=1$, $k_2=5$, $\tilde{\sigma}_2=3$, $\tilde{\sigma}_3=1$, $\eta_2=0.5$, $\eta_3=0.5$, $\theta=60$, $\hat{\rho}_1=1$, $\hat{\rho}_3=2$, $W_1=8$ and $W_2=10$ with $\tilde{\sigma}_1=2, 10$ and 18 of the partitions (a), (b) and (c), respectively.

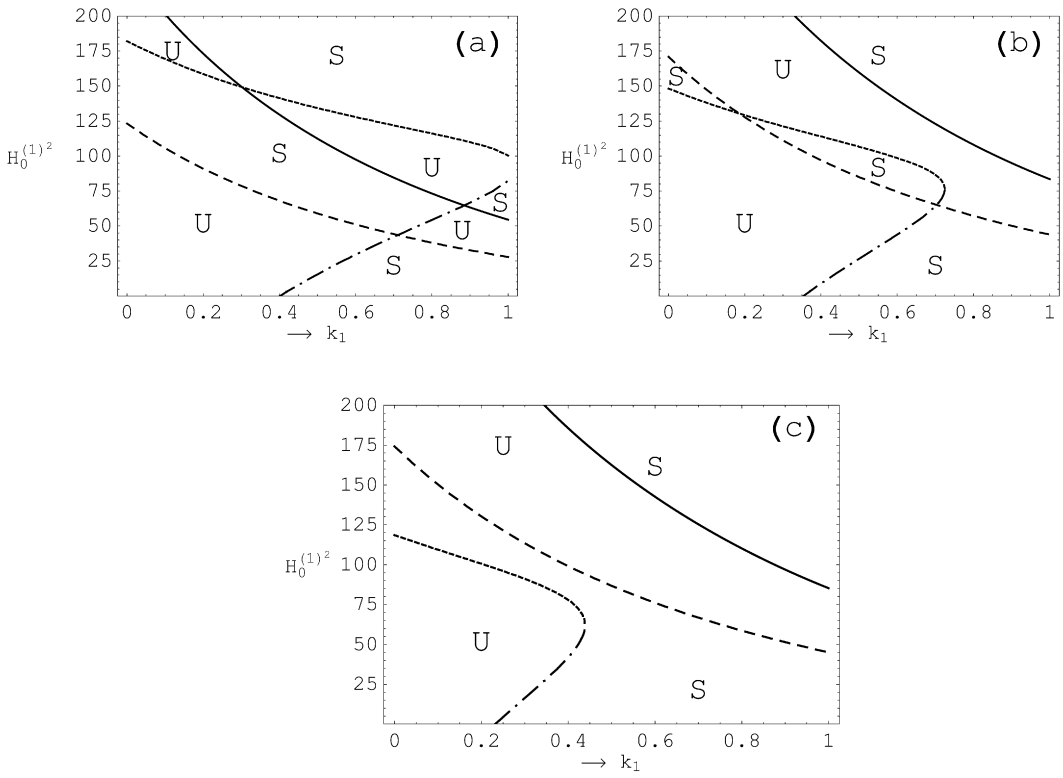

Fig. 6. Represents the stability diagrams in the plane ($H_0^{(1)^2}$–k_1), according to relations (25) for a system having $H_0^{(2)} = 10$, $H_0^{(3)} = 5$, $U_1^{(1)} = 0.01$, $U_2^{(1)} = 0.02$, $U_1^{(2)} = 4.3$, $U_2^{(2)} = 2.5$, $U_1^{(3)} = 0.85$, $U_2^{(3)} = 0.5$, $k_2 = 5$, $\tilde{\sigma}_1 = 0.1$, $\tilde{\sigma}_2 = 3$, $\tilde{\sigma}_3 = 0.2$, $\eta_1 = 0.02$, $\eta_3 = 0.005$, $\theta = 60$, $\hat{\rho}_1 = 10$, $\hat{\rho}_3 = 20$, $W_1 = 8$ and $W_2 = 10$ with $\eta_2 = 0.01, 0.3$ and 0.4 of the partitions (a), (b) and (c), respectively.

(28) reveals that there are five regions in the plane ($H_0^{(1)^2}$–η_1). For the parts (b) and (c) of Fig. 5, we select the values of the porosity as $\tilde{\sigma}_1 = 10, 18$ respectively. It is shown that the increasing of the porosity leads to an increase of the stable regions while it leads to a contraction in the unstable areas. At this end, it can be demonstrated that the increase of the porosity has a stabilizing effect in the stability behavior. On other meaning, the increase in the porosity sometimes damps the surface waves where a part of its kinetic energy may be absorbed, and hence stabilizing role is found. The effect of the increase of the viscosity coefficient of the intermediate layer on the stability behavior is displayed in Fig. 6. The graphs shown in the plane ($H_0^{(1)^2}$–k_1) are achieved for three values of the viscosity $\eta_2 = 0.01, 0.3$ and 0.4, where the other quantities are held fixed as $H_0^{(2)} = 10$, $H_0^{(3)} = 5$, $U_1^{(1)} = 0.01$, $U_2^{(1)} = 0.02$, $U_1^{(2)} = 4.3$, $U_2^{(2)} = 2.5$, $U_1^{(3)} = 0.85$, $U_2^{(3)} = 0.5$, $k_2 = 5$, $\tilde{\sigma}_1 = 0.1$, $\tilde{\sigma}_2 = 3$, $\tilde{\sigma}_3 = 0.2$, $\eta_1 = 0.02$, $\eta_3 = 0.005$, $\theta = 60$, $\hat{\rho}_1 = 10$, $\hat{\rho}_3 = 20$, $W_1 = 8$ and $W_2 = 10$. In this case, the plane ($H_0^{(1)^2} - k_1$) is partitioned to stable and unstable regions where the stability configuration is controlled by conditions (25). The stability pictures in Fig. 6 (parts (a), (b) and (c)) show that the increase of the viscosity coefficient η_2 implies that the stable regions are increased while the unstable regions are decreased. Thus, we conclude that the viscosity coefficient η_2 plays a stabilizing role in the movement of the waves in the inner layer of the fluid sheet.

4. Instability of one interface between two conducting fluids

The goal of this section is to investigate the limiting case when the thickness of the inner layer tends to zero (i.e. $a \to 0$). Define the dimensionless length as $\sqrt{T/g\rho_2}$ (since for any physical quantities defined above the medium 3 tends to the medium 2, for example, $\rho_3 \to \rho_2$, $\tilde{\sigma}_3 \to \tilde{\sigma}_2$). At this stage the dispersion equation, which controls the Kelvin–Helmholtz instability of the interface between the two superimposed conducting fluids, is

$$\omega^2 + (\beta_1 + i\beta_2)\omega + \beta_3 + i\beta_4 = 0, \tag{30}$$

where the coefficients that appeared in this equation are given in Appendix A(IV). Relation (30) is quadratic equation in ω with complex coefficients. The system characterized by (30) will be stable when [32]

$$\beta_1 \geqslant 0,$$
$$\beta_1(\beta_1\beta_3 + \beta_2\beta_4) - \beta_4^2 > 0. \tag{31}$$

The first condition of (31) is always satisfied and hence, conditions (31) can be rewritten in the form

$$\tilde{\beta}_1 U_2^{(2)^2} + \tilde{\beta}_2 U_2^{(2)} + \tilde{\beta}_3 > 0, \tag{32}$$

where the coefficients $\tilde{\beta}_j$ $(j = 1, 2, 3)$ are given in Appendix A(V).

In Figs. 7–9, our goal is to determine the numerical profiles for the stability pictures of the surface waves propagating through the interface, which separates two superposed conducting fluid layers through porous media. In order to screen this examination, numerical calculations for the stability condition (32) are achieved for the variation of the physical parameters k_1, k_2, η_1 and $\tilde{\sigma}_2$. The influence of the streaming of the fluid in the stability criteria for the motion of waves is the aim of the calculations depicted in Fig. 7. This graph represents the transition curves of condition (32), in the plane ($U_2^{(2)^2}$–k_1), corresponding to three different values of the stream velocity $U_1^{(2)} = 12, 30, 50$ of the parts (a), (b) and (c), respectively, and for a system having the physical parameters $H_0^{(1)} = 10$, $H_0^{(2)} = 15$, $U_1^{(1)} = 12$, $U_2^{(1)} = 10$, $k_2 = 5$, $\tilde{\sigma}_1 = 5$, $\tilde{\sigma}_2 = 3$, $\eta_2 = 5$, $\theta = 30$, $\hat{\rho}_1 = 0.1$ and $W = 8$. In Fig. 7(a) the plane ($U_2^{(2)^2}$–k_1) is divided into one unstable and two stable regions.

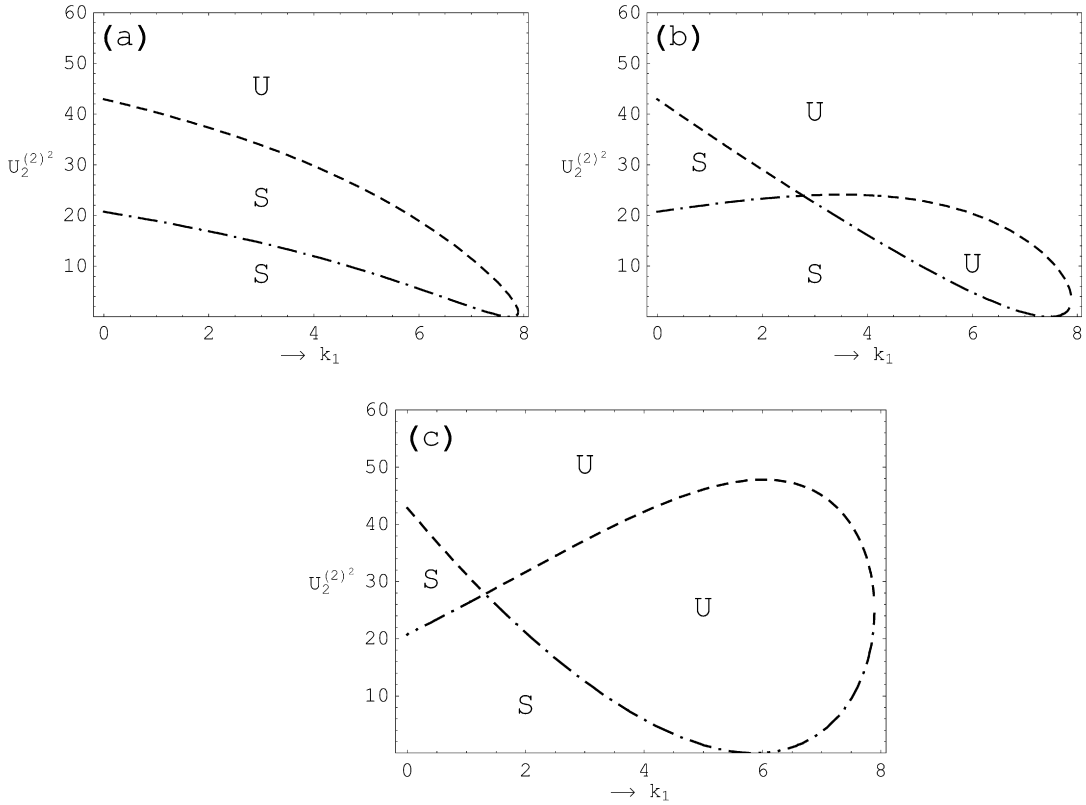

Fig. 7. The transition curves in the plane $(U_2^{(2)^2}$–$k_1)$ based on relations (32), for a system having $H_0^{(1)} = 10$, $H_0^{(2)} = 15$, $U_1^{(1)} = 12$, $U_2^{(1)} = 10$, $k_2 = 5$, $\tilde{\sigma}_1 = 5$, $\tilde{\sigma}_2 = 3$, $\eta_2 = 5$, $\theta = 30$, $\hat{\rho}_1 = 0.1$ and $W = 8$ with $U_1^{(2)} = 12, 30, 50$ of the partitions (a), (b) and (c), respectively.

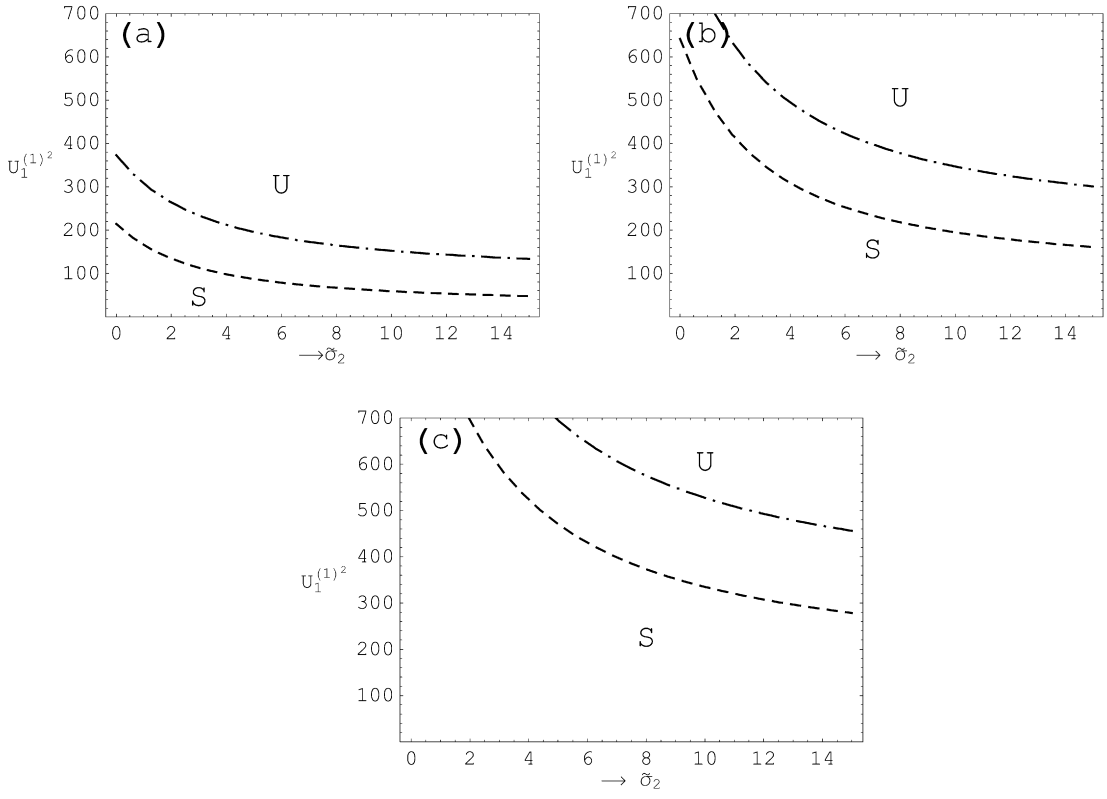

Fig. 8. The stability diagrams in the plane $(U_1^{(1)^2}$–$\tilde{\sigma}_2)$ according to relations (32), for a system having $H_0^{(1)} = 8$, $U_2^{(1)} = 2$, $U_1^{(2)} = 3$, $U_2^{(2)} = 1$, $k_1 = 1.5$, $k_2 = 1$, $\tilde{\sigma}_1 = 5$, $\eta_1 = 0.1$, $\eta_2 = 0.5$, $\theta = 30$, $\hat{\rho}_1 = 10$ and $W = 8$ with $H_0^{(2)} = 20, 45$ and 60 of the partitions (a), (b) and (c), respectively.

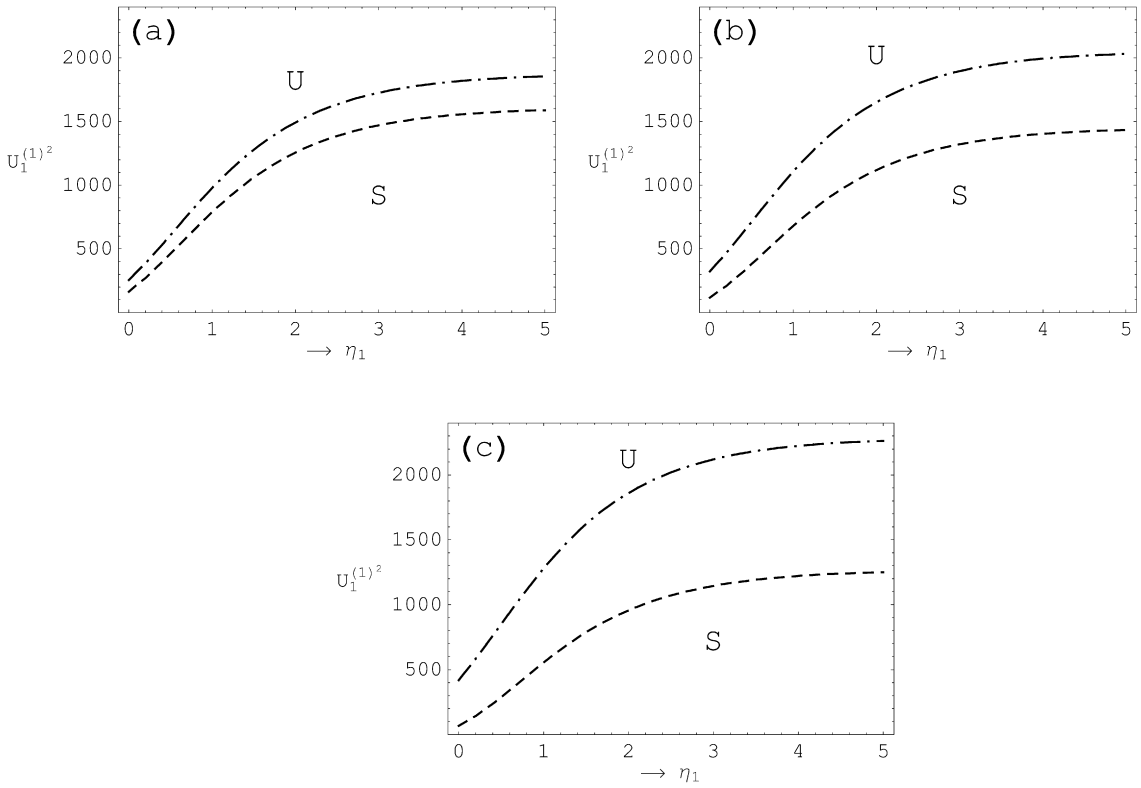

Fig. 9. The graph is constructed for $U_1^{(1)^2}$ versus η_1, for a system having the parameters $H_0^{(1)} = 18$, $H_0^{(2)} = 15$, $U_2^{(1)} = 2$, $U_1^{(2)} = 6$, $k_1 = 1$, $k_2 = 5$, $\tilde{\sigma}_1 = 5$, $\tilde{\sigma}_2 = 8$, $\theta = 45$, $\eta_2 = 0.5$, $\hat{\rho}_1 = 10$ and $W = 8$ with $U_2^{(2)} = 4, 8$ and 13 of the partitions (a), (b) and (c), respectively.

The parts (b) and (c) are plotted at the values $U_1^{(2)} = 30, 50$, respectively. We found that the plane is partitioned to four areas of stability and instability. An inspection of the stability chart reveals that, broadly speaking, the increase of the stream velocity leads to an extension in the width of the unstable area. It is worthwhile to notice that the destabilizing effect of the stream can be observed. In other words, the increase in the velocity sometimes damps the surface waves where a part of its kinetic energy may be absorbed, while it excites them in others due to the increase of this energy. Further, we observe that the variation of the profile shape of the interacting surface waves is not regular. The examination of change of magnetic field in the stability criteria is illustrated in the $(U_1^{(1)^2} - \tilde{\sigma}_2)$ plane throughout the parts of Fig. 8. The calculations displayed in Fig. 8 are made for a system having $H_0^{(1)} = 8$, $U_2^{(1)} = 2$, $U_1^{(2)} = 3$, $U_2^{(2)} = 1$, $k_1 = 1.5$, $k_2 = 1$, $\tilde{\sigma}_1 = 5$, $\eta_1 = 0.1$, $\eta_2 = 0.5$, $\theta = 30$, $\hat{\rho}_1 = 10$ and $W = 8$, while the field $H_0^{(2)}$ has three different values $(= 20, 45, 60)$ for the sake of comparison. It is found that the stability diagram has two transition curves that divide it into three regions. An inspection of the stability diagrams of Fig. 8 reveals that the increase of the magnetic field leads to an increase in the width of the of unstable region, and more contraction in the width of the stable regions. Thus, we conclude that the increase of the magnetic field has a destabilizing role. However, it is to be expected that a more careful search would clarify that the motion of the interfacial waves will be more irregular and perturbed with the increase of the values of the magnetic field. In other words, when the magnetic field is increased, the field sometimes keeps its energy and absorbs a part of the kinetic energy of the interfacial waves, while it transmits its energy to these waves, which leads to the instability in the motion of the waves. Fig. 9 shows the effect of the increasing velocity in the plane $(U_1^{(1)^2} - \eta_1)$ for a system having $H_0^{(1)} = 18$, $H_0^{(2)} = 15$, $U_2^{(1)} = 2$, $U_1^{(2)} = 6$, $k_1 = 1$, $k_2 = 5$, $\tilde{\sigma}_1 = 5$, $\tilde{\sigma}_2 = 8$, $\theta = 45$, $\eta_2 = 0.5$, $\hat{\rho}_1 = 10$ and $W = 8$, where part (a) is plotted at the value $U_2^{(2)} = 4$, and the values $U_2^{(2)} = 8, 13$ for the parts (b) and (c), respectively. Having noted the stability chart of these diagrams, it is observed that further increasing of the velocity in the upper layer leads to further increase in the width of unstable regions, and more contraction in the width of the stable region simultaneously. A conclusion that may be made here is that the velocity has a stabilizing influence on the stability behavior of the surface waves.

5. Conclusions

The linear stability of a three superposed conducting fluids in three-dimensional motion through porous media has been studied. The fluids are incompressible and perfectly conducting and there are weak viscous stresses on the interfaces. The stability conditions of the Rayleigh–Taylor problem and the Kelvin–Helmholtz problem have been investigated. We conclude that for the Rayleigh–Taylor problem and the Kelvin–Helmholtz instability develops in a Darcian flow, the fluid properties must meet certain conditions. In this respect, the Rayleigh–Taylor problem (nonstreaming) and the Kelvin–Helmholtz instability for flow in porous media differ from the instability in continuum flow was the occurrence of the instability depends on the magnitude of the velocities alone. In the general case of the Kelvin–Helmholtz instability, the solution of the system leads to a dispersion relation of fourth degree with complex coefficients which contains the most stability information of MHD flow (in the case of the Rayleigh–Taylor problem the dispersion relation has real coefficients). In the limiting case of one interface, we obtain quadratic dispersion relation with complex coefficients.

Numerical estimations are made where the physical parameters are put in the dimensionless form. Some stability diagrams

are plotted and discussed. The stability examination yields the following results:

(i) According to the numerical example, for the Rayleigh–Taylor problem we remark that the viscosity coefficients play a stabilizing role in both of the movement of the upper and the lower layers of the fluids. This regular influence may be physically interpreted as apart of the kinetic energy of the waves has been absorbed, which leads to damping in the frequency of the waves.

(ii) In the case of the Kelvin–Helmholtz problem, the numerical calculations show the following: the variation of the velocity in the inner layer of the fluids plays a destabilizing role in the movement of the fluids, while the viscosity coefficient in the intermediate layer plays a stabilizing role in the movement of the fluid sheet. In addition, the stability behavior is noticed for the increasing of the porosity in the upper layer. In other words, the increase in the porosity sometimes damps the surface waves where a part of its kinetic energy may be absorbed.

(iii) Numerical applications of instability of one interface as a special case illustrated that the increase of the magnetic field has a destabilizing role. On other meaning, when the magnetic field is increased, the field sometimes keeps its energy and absorbs a part of the kinetic energy of the interfacial waves, while it transmits its energy to these waves, which leads to the instability in the motion of the waves.

Appendix A

(I) The formulas for the quantities, which are used in Eq. (18) are

$$\begin{aligned}
A_1^{(1)} &= k^{-1}\{e^k\omega^2 + e^k[\hat{\rho}_1^{-1}\tilde{\sigma}_1 + 2i(k_1U_1^{(1)} + k_2U_2^{(1)})]\omega \\
&\quad + e^k H_0^{(1)^2}(k_1\cos\theta + k_2\sin\theta)^2 - (k_1U_1^{(1)} + k_2U_2^{(1)})^2 \\
&\quad + ie^k\hat{\rho}_1^{-1}\tilde{\sigma}_1(k_1U_1^{(1)} + k_2U_2^{(1)})\}\hat{\xi}_1,
\end{aligned}$$

$$\begin{aligned}
A_2^{(3)} &= -k^{-1}\{e^k\omega^2 + e^k[\hat{\rho}_3^{-1}\tilde{\sigma}_3 + 2i(k_1U_1^{(3)} + k_2U_2^{(3)})]\omega \\
&\quad + e^k H_0^{(1)^2}(k_1\cos\theta + k_2\sin\theta)^2 - (k_1U_1^{(3)} + k_2U_2^{(3)})^2 \\
&\quad + ie^k\hat{\rho}_3^{-1}\tilde{\sigma}_3(k_1U_1^{(3)} + k_2U_2^{(3)})\}\hat{\xi}_2,
\end{aligned}$$

$$\begin{aligned}
A_1^{(2)} &= (1-e^{4k})^{-1}k^{-1}e^k\{\omega^2 + [\tilde{\sigma}_2 + 2i(k_1U_1^{(2)} + k_2U_2^{(2)})]\omega \\
&\quad + H_0^{(2)^2}(k_1\cos\theta + k_2\sin\theta)^2 \\
&\quad - (k_1U_1^{(2)} + k_2U_2^{(2)})^2 + i\tilde{\sigma}_2(k_1U_1^{(2)} + k_2U_2^{(2)})\}\hat{\xi}_1 \\
&\quad + (1-e^{4k})^{-1}k^{-1}e^{3k}\{\omega^2 - [\tilde{\sigma}_2 + 2i(k_1U_1^{(2)} + k_2U_2^{(2)})]\omega \\
&\quad - H_0^{(2)^2}(k_1\cos\theta + k_2\sin\theta)^2 \\
&\quad + (k_1U_1^{(2)} + k_2U_2^{(2)})^2 - i\tilde{\sigma}_2(k_1U_1^{(2)} + k_2U_2^{(2)})\}\hat{\xi}_2,
\end{aligned}$$

$$\begin{aligned}
A_2^{(2)} &= (1-e^{4k})^{-1}k^{-1}e^{3k}\{\omega^2 + [\tilde{\sigma}_2 + 2i(k_1U_1^{(2)} + k_2U_2^{(2)})]\omega \\
&\quad + H_0^{(2)^2}(k_1\cos\theta + k_2\sin\theta)^2 - (k_1U_1^{(2)} + k_2U_2^{(2)})^2 \\
&\quad + i\tilde{\sigma}_2(k_1U_1^{(2)} + k_2U_2^{(2)})\}\hat{\xi}_1 + (1-e^{4k})^{-1}k^{-1}e^k \\
&\quad \times\{\omega^2 - [\tilde{\sigma}_2 + 2i(k_1U_1^{(2)} + k_2U_2^{(2)})]\omega \\
&\quad - H_0^{(2)^2}(k_1\cos\theta + k_2\sin\theta)^2 \\
&\quad + (k_1U_1^{(2)} + k_2U_2^{(2)})^2 - i\tilde{\sigma}_2(k_1U_1^{(2)} + k_2U_2^{(2)})\}\hat{\xi}_2.
\end{aligned}$$

(II) The calculations of the coefficients of Eq. (23) are

$$\begin{aligned}
\alpha_1 &= (1/L_0)(L_{11}L_{22} + L_{12}L_{22} - M_{11}M_{22} - M_{12}M_{21}), \\
\alpha_2 &= (1/L_0)(L_{11}L_{23} + L_{13}L_{21} - M_{11}M_{23} - M_{13}M_{21}), \\
\alpha_3 &= (1/L_0)(L_{11}L_{24} + L_{12}L_{22} + L_{14}L_{21} - L_{13}L_{23} + M_{13}M_{23} \\
&\quad - M_{11}M_{24} - M_{12}M_{22} - M_{14}M_{21}), \\
\alpha_4 &= (1/L_0)(L_{15}L_{21} + L_{13}L_{22} + L_{12}L_{23} + L_{11}L_{25} - M_{10}M_{21} \\
&\quad - M_{13}M_{22} - M_{12}M_{23} - M_{11}M_{25}), \\
\alpha_5 &= (1/L_0)(L_{12}L_{24} + L_{14}L_{22} - L_{15}L_{23} - L_{13}L_{25} \\
&\quad + M_{13}M_{25} + M_{15}M_{23} - M_{12}M_{24} - M_{14}M_{22}), \\
\alpha_6 &= (1/L_0)(L_{13}L_{24} + L_{14}L_{23} + L_{15}L_{22} + L_{12}L_{25} \\
&\quad - M_{10}M_{22} - M_{12}M_{25} - M_{13}M_{24} - M_{14}M_{23}), \\
\alpha_7 &= (1/L_0)(L_{14}L_{24} - L_{15}L_{25} + M_{10}M_{25} - M_{14}M_{24}), \\
\alpha_8 &= (1/L_0)(L_{14}L_{25} + L_{15}L_{24} - M_{15}M_{24} - M_{14}M_{25}), \\
L_0 &= L_{11}L_{21} - M_{11}M_{21},
\end{aligned}$$

where

$$\begin{aligned}
L_{11} &= -\frac{\hat{\rho}_1(1-e^{4k}) - (1+e^{4k})}{k(1-e^{4k})}, \\
L_{21} &= -\frac{\hat{\rho}_3(1-e^{4k}) - (1+e^{4k})}{k(1-e^{4k})}, \\
L_{12} &= \frac{(1+e^{4k})(2k^2\eta_2 + \tilde{\sigma}_2) - (1-e^{4k})(2k^2\eta_1 + \tilde{\sigma}_1)}{k(1-e^{4k})}, \\
L_{22} &= \frac{(1+e^{4k})(2k^2\eta_3 + \tilde{\sigma}_3) - (1-e^{4k})(2k^2\eta_2 + \tilde{\sigma}_2)}{k(1-e^{4k})}, \\
L_{13} &= \frac{2}{k(1-e^{4k})}\{k_1[U_1^{(2)}(1+e^{4k}) - \hat{\rho}_1U_1^{(1)}(1-e^{4k})] \\
&\quad + k_2[U_2^{(2)}(1+e^{4k}) - \hat{\rho}_1U_2^{(1)}(1-e^{4k})]\}, \\
L_{23} &= \frac{2}{k(1-e^{4k})}\{k_1[U_1^{(2)}(1+e^{4k}) - \hat{\rho}_3U_1^{(3)}(1-e^{4k})] \\
&\quad + k_2[U_2^{(2)}(1+e^{4k}) - \hat{\rho}_3U_2^{(3)}(1-e^{4k})]\}, \\
L_{14} &= \frac{1}{k(1-e^{4k})}\{k_2[k_2\hat{\rho}_1U_2^{(1)^2}(1-e^{4k}) + 2k_1[\hat{\rho}_1U_1^{(1)}U_2^{(1)}(1-e^{4k}) \\
&\quad - U_1^{(2)}U_2^{(2)}(1+e^{4k})]] + k(1-e^{4k})(\hat{\rho}_1 + k_2^2W_1 - 1) \\
&\quad - (1+e^{4k})[k_2^2U_2^{(2)^2} + 2H_0^{(2)^2}(k_1\cos\theta + k_2\sin\theta)^2 \\
&\quad - 2\hat{\rho}_1k_2H_0^{(1)^2}(1-e^{4k})(k_1\sin 2\theta + k_2\sin^2\theta) \\
&\quad - k_1^2[U_1^{(2)^2}(1+e^{4k}) - (1-e^{4k})(kW_1 + \hat{\rho}_1(U_1^{(1)^2} \\
&\quad - 2H_0^{(1)^2}\cos^2\theta)]]\}, \\
L_{24} &= \frac{1}{k(1-e^{4k})}\{k_2[k_2\hat{\rho}_3U_2^{(1)^2}(1-e^{4k}) + 2k_1[\hat{\rho}_3U_3^{(1)}U_2^{(1)}(1-e^{4k}) \\
&\quad - U_3^{(2)}U_2^{(2)}(1+e^{4k})]] - k(1+e^{4k})(\hat{\rho}_3 + k_2^2W_2 - 1) \\
&\quad - (1+e^{4k})[k_2^2U_2^{(2)^2} + 2H_0^{(2)^2}(k_1\cos\theta + k_2\sin\theta)^2 \\
&\quad - 2\hat{\rho}_3k_2H_0^{(3)^2}(1-e^{4k})(k_1\sin 2\theta + k_2\sin^2\theta) \\
&\quad - k_1^2[U_1^{(2)^2}(1+e^{4k}) - (1+e^{4k})(kW_2 \\
&\quad + \hat{\rho}_3(U_1^{(3)^2} - 2H_0^{(3)^2}\cos^2\theta)]]\}, \\
L_{15} &= -\frac{1}{k(1-e^{4k})}\{(1-e^{4k})(2k^2\eta_1 + \tilde{\sigma}_1)(k_1U_1^{(1)} + k_2U_2^{(1)}) \\
&\quad - (1+e^{4k})(2k^2\eta_2 + \tilde{\sigma}_2)(k_1U_1^{(2)} + k_2U_2^{(2)})\},
\end{aligned}$$

$$L_{25} = -\frac{1}{k(1-e^{4k})}\{(1-e^{4k})(2k^2\eta_3+\tilde{\sigma}_3)(k_1U_1^{(3)}+k_2U_2^{(3)}) - (1+e^{4k})(2k^2\eta_2+\tilde{\sigma}_2)(k_1U_1^{(2)}+k_2U_2^{(2)})\},$$

$$M_{11} = M_{21} = -\frac{2e^{2k}}{k(1-e^{4k})},$$

$$M_{12} = M_{22} = M_{11}(2k^2\eta_2+\tilde{\sigma}_2),$$

$$M_{13} = M_{11}(k_1U_1^{(2)}+k_2U_2^{(2)}),$$

$$M_{14} = M_{24} = M_{11}\{2H_0^{(2)^2}(k_1\cos\theta+k_2\sin\theta)^2 - (k_1U_1^{(2)}+k_2U_2^{(2)})^2\},$$

$$M_{15} = M_{25} = M_{12}(k_1U_1^{(2)}+k_2U_2^{(2)}).$$

(III) The values of κ_j which are used in Eq. (24) are

$$\kappa_1 = \alpha_1, \qquad \kappa_2 = \alpha_1(\alpha_1\alpha_3+\alpha_2\alpha_4-\alpha_5)-\alpha_4^2,$$

$$\kappa_3 = \kappa_2(\alpha_1(\alpha_3\alpha_5+\alpha_4\alpha_6-\alpha_1\alpha_7-\alpha_2\alpha_8)-\alpha_5^2) - (\alpha_1(\alpha_1\alpha_6-\alpha_2\alpha_5)+\alpha_4\alpha_5-\alpha_1\alpha_8)^2,$$

$$\kappa_4 = \kappa_{41}\kappa_{42}-\kappa_{43}^2,$$

$$\kappa_{41} = \kappa_2(\alpha_1(\alpha_5\alpha_7+\alpha_6\alpha_8)-\alpha_8^2)-(\alpha_1(\alpha_1\alpha_7+\alpha_2\alpha_8)-\alpha_4\alpha_8)^2,$$

$$\kappa_{42} = \kappa_2(\alpha_1(\alpha_3\alpha_5+\alpha_4\alpha_6)-\alpha_1(\alpha_1\alpha_7-\alpha_2\alpha_8)-\alpha_5^2) - (\alpha_1(\alpha_1\alpha_6-\alpha_2\alpha_5)-\alpha_1\alpha_8+\alpha_4\alpha_5)^2,$$

$$\kappa_{43} = \kappa_2(\alpha_1(\alpha_3\alpha_8-\alpha_4\alpha_7)-\alpha_5\alpha_8)+(\alpha_1(\alpha_1\alpha_7+\alpha_2\alpha_8)-\alpha_4\alpha_8) \times(\alpha_1(\alpha_1\alpha_6-\alpha_2\alpha_5)-\alpha_1\alpha_8+\alpha_5\alpha_4).$$

(IV) The quantities given in Eq. (30) are defined as

$$\beta_1 = \frac{2k^2(\eta_1+\eta_2)+\tilde{\sigma}_1+\tilde{\sigma}_2}{1+\hat{\rho}_1},$$

$$\beta_2 = \frac{2[k_1(\hat{\rho}_1U_1^{(1)}+U_1^{(2)})+k_2(\hat{\rho}_1U_2^{(1)}+U_2^{(2)})]}{1+\hat{\rho}_1},$$

$$\beta_3 = \frac{1}{1+\hat{\rho}_1}\{k(1-\hat{\rho}_1)-k_1^2[kW+\hat{\rho}_1U_1^{(1)^2}+U_1^{(2)^2} - 2\cos^2\theta(H_0^{(2)^2}-2\hat{\rho}_1H_0^{(1)^2})]-k_2^2[kW+\hat{\rho}_1U_1^{(1)^2}+U_1^{(2)^2} - 2\sin^2\theta(H_0^{(2)^2}-2\hat{\rho}_1H_0^{(1)^2})]+2k_1k_2[\hat{\rho}_1(H_0^{(1)^2}\sin2\theta - U_1^{(1)^2}U_2^{(1)^2})+H_0^{(2)^2}\sin2\theta-U_1^{(2)^2}U_2^{(2)^2}]\},$$

$$\beta_4 = \frac{(2k^2\eta_1+\tilde{\sigma}_1)\{k_1U_1^{(1)}+k_2U_2^{(1)}\}+(2k^2\eta_2+\tilde{\sigma}_2)\{k_1U_1^{(2)}+k_2U_2^{(2)}\}}{1+\hat{\rho}_1}.$$

(V) The algebraic formulas involved in relation (32) are

$$\tilde{\beta}_1 = -k_2^2[\tilde{\sigma}_1^2+4k^2\eta_1(\eta_1+\tilde{\sigma}_1)+\hat{\rho}_1(2k^2\eta_2+\tilde{\sigma}_2)^2],$$

$$\tilde{\beta}_2 = -2\tilde{\beta}_1k_2^{-1}[k_1(U_1^{(1)}-U_1^{(2)})+k_2U_2^{(1)}],$$

$$\tilde{\beta}_3 = k(\tilde{\sigma}_1+\tilde{\sigma}_2)^2+kW\tilde{\sigma}_1^2(k_1^2+k_2^2)-2\tilde{\sigma}_1k_1^2H_0^{(2)^2}\cos^2\theta(\tilde{\sigma}_1+2\tilde{\sigma}_2) - 2k_2\tilde{\sigma}_1H_0^{(2)^2}\sin^2\theta(k_2\tilde{\sigma}_1+k_1\tilde{\sigma}_2)-k_1\tilde{\sigma}_1^2U_1^{(1)}(k_1U_1^{(2)}+k_2U_2^{(1)}) + (\tilde{\sigma}_1^2+\hat{\rho}_1\tilde{\sigma}_2^2)(k_1U_1^{(2)}-k_2U_2^{(1)})^2-2\hat{\rho}_1H_0^{(1)^2}[k_1\cos\theta + k_2\sin\theta](\tilde{\sigma}_1+\tilde{\sigma}_2)^2+(4k^4\eta_1^2+\tilde{\sigma}_1)[k^3W+k(\hat{\rho}_1-1) + k_1^2(U_1^{(1)}-U_1^{(2)})^2-2k_1k_2U_2^{(1)}(U_1^{(1)}-U_1^{(2)}) + k_2^2U_2^{(1)^2}-2(\hat{\rho}_1H_0^{(1)^2}+H_0^{(2)^2})(k_1\cos\theta+k_2\sin\theta)^2] + (4k^4\eta_2^2+\tilde{\sigma}_2)[k^3W+k(\hat{\rho}_1-1)+\hat{\rho}_1k_1^2(U_1^{(1)}-U_1^{(2)})^2 - 2\hat{\rho}_1k_1k_2U_2^{(1)}(U_1^{(1)}-U_1^{(2)})+\rho_1k_2^2U_2^{(1)^2}-2(\hat{\rho}_1H_0^{(1)^2} + H_0^{(2)^2})(k_1\cos\theta+k_2\sin\theta)^2]+(\tilde{\sigma}_1+\tilde{\sigma}_2)[k^3W+k(\hat{\rho}_1-1) - 2(\hat{\rho}_1H_0^{(1)^2}+H_0^{(2)^2})(k_1\cos\theta+k_2\sin\theta)^2].$$

References

[1] S. Chandrasekhar, Hydrodynamic and Hydromagnetic Stability, Oxford Univ. Press, Oxford, 1961.
[2] J.F. Lyon, The electrohydrodynamic Kelvin–Helmholtz instability, S.M. thesis, Department of Electrical Engineering, MIT, Cambridge, MA, 1962.
[3] J.R. Melcher, Field Coupled Surface Waves, MIT Press, Cambridge, MA, 1963; J.R. Melcher, Continuum Electromechanics, MIT Press, Cambridge, MA, 1981.
[4] S.K. Malik, M. Singh, Nonlinear focusing and the Kelvin–Helmholtz instability in ferrofluid nonmagnetic fluid systems, Phys. Fluids 31 (1988) 1069.
[5] W.C. Chin, Wave Propagation in Petroleum Engineering, Gulf Publishing Company, Houston, USA, 1994.
[6] A. Klinkenberg, J.L. Van der Minne, Electrostatics in the Petroleum Industry, Elsevier, Amsterdam, 1958.
[7] R.C. Sharma, K.P. Thakur, Instability through porous medium of two viscous superposed conducting fluids, Internat. J. Math. Sci. 5 (2) (1982) 365.
[8] D.A. Nield, A. Bejan, Convection in Porous Media, Springer-Verlag, New York, 1992.
[9] D.B. Ingham, I. Pop (Eds.), Transport Phenomena in Porous Media, Pergamon Press, Oxford, 1998.
[10] K. Vafai (Ed.), Handbook of Porous Media, Marcel Dekker, New York, 2000.
[11] I. Pop, D.B. Ingham, Convective Heat Transfer: Mathematical and Computational Modeling of Viscous Fluids and Porous Media, Pergamon Press, Oxford, 2001.
[12] Sunil, R.C. Sharma, R.S. Chandel, On superposed coupled-stress fluids in porous medium in hydromagnetics, Z. Naturforsch. 57a (2002) 955.
[13] St.I. Gheorghitza, The generalization of some results concerning the Kelvin–Helmholtz instability, J. Sci. Eng. Res. 13 (1969) 39.
[14] A. Georgescu, St.I. Gheorghitza, On the Kelvin–Helmholtz instability in presence of porous media, Rev. Roum. Math. Pure Appl. 14 (1971) 27.
[15] K. Zakaria, M.A. Sirwah, S. Alkharashi, Temporal stability of superposed magnetic fluids in porous media, Phys. Scripta 77 (2008) 1.
[16] M.F. El-Sayed, Electrohydrodynamic instability of dielectric fluid layer between two semi-infinite identical conducting fluids in porous medium, Physica A 367 (2006) 25.
[17] M.F. El-Sayed, The effects of collisions with neutral particles on the instability of two superposed composite plasmas streaming through porous medium, Z. Naturforsch. 45a (1999) 411.
[18] S. Korsunsky, Long waves on a thin layer of conducting fluid flowing down an inclined plane in an electromagnetic field, Eur. J. Mech. B/Fluids 18 (2) (1999) 295.
[19] Sunil, P. Singh, Thermal instability of a porous medium with relaxation and inertia in the presence of Hall effects, Archive of Applied Mechanics 70 (2000) 649.
[20] H.A. Attia, M.E. Sayed-Ahmed, Hall effect on unsteady MHD Couette flow and heat transfer of a Bingham fluid with suction and injection, Applied Mathematical Modelling 28 (2004) 1027.
[21] E.A. Pushkar, Gasdynamic analogies in problems of the oblique interaction of MHD shock waves, Fluid Dynamics 36 (6) (2001) 989 (translated from Izvestiya Rossiiskoi Academii Nauk, Mekhanika Zhidkosti i Gaza).
[22] K.I. Ilin, Y.L. Trakhinin, V.A. Vladimirov, The stability of steady MHD flows with current-vortex sheets, Phys. Plasmas 10 (2003) 2649.
[23] A. Blokhin, Yu. Trakhinin, Stability of Strong Discontinuities in Magnetohydrodynamics and Electrohydrodynamics, Nova Science Publishers, New York, 2003.
[24] T. Shirota, Regularity of solutions to mixed problems of linearized MHD equations, Nara Women's University. Koukyuroku in Math. 1 (1994) 1 (in Japanese).
[25] G.K. Batchelor, An Introduction to Fluid Dynamics, Cambridge University Press, 1967.
[26] D. Halliday, R. Resnick, J. Walker, Fundamentals of Physics, John Wiley & Sons, 1997.
[27] H.H. Woodson, J.R. Melcher, Electromechanical Dynamics, John Wiley & Sons, 1968.
[28] L.D. Landau, E.M. Lifshitz, Electrohydrodynamics of Continuous Media, Pergamon Press, Oxford, 1960.
[29] P.M. Adler, Porous Media, Butterworth–Heineman, London, 1992.
[30] F.A.L. Dullien, Porous Media, Academic Press, New York, 1992.
[31] E.N. Parker, Interplanetary Dynamical Processes, Interscience, New York, 1963.
[32] H. Leipholz, Stability Theory: An Introduction to the Stability of Dynamic Systems and Rigid Bodies, Wiley and Teubner, Stuttgart, 1987.